

Effect of stoichiometry on the structure of $\text{TiO}_2(110)$

P. W. Murray, N. G. Condon, and G. Thornton*

Interdisciplinary Research Centre in Surface Science, University of Liverpool, Liverpool L69 3BX, United Kingdom

(Received 2 September 1994)

Scanning tunneling microscopy has been used to investigate the structure of $\text{TiO}_2(110)$ as a function of oxygen-vacancy density. The results are consistent with imaging Ti atoms, as expected given the positive sample bias employed. Our results for the stoichiometric 1×1 surface are in line with the structure expected on the basis of bulk termination. On the surfaces prepared here, a small density of the reduced 1×2 phase always accompanied the 1×1 termination, nucleating at step edges. With increasing O-vacancy density, the 1×2 phase increased in area, eventually dominating the surface. Atomically resolved images indicate a structure that involves the loss of every other bridging O row, a 0.5-Å lateral displacement of fivefold-coordinated Ti atoms along $[\bar{1}\bar{1}0]$, and a relaxation of Ti^{3+} ions towards the bulk. Coexisting with the 1×2 phase is a structure with 2×2 local symmetry that is periodic along $[\bar{1}\bar{1}0]$. This appears to arise from a transfer of O from the remaining bridging O rows to reoccupy O-vacancy sites and to sit atop fivefold-coordinated Ti atoms. Accompanying this rearrangement of O atoms, fivefold Ti atoms relax back to their positions in the 1×1 phase, suggesting that the 2×2 phase acts to relieve the strain imposed by formation of the 1×2 morphology. Further reduction of the substrate results in faceting to (100), (011), and (111) planes.

I. INTRODUCTION

Transition-metal oxides are important in several areas of technology, such as gas sensing and catalysis, with the surface properties being crucial to many of these applications. TiO_2 , for example, is a model photocatalyst for the dissociation of water.¹ Work related to this and related processes has given rise to a substantial database on the surface science of TiO_2 .² In this paper we describe a scanning tunneling microscopy study of stoichiometric and nonstoichiometric phases of $\text{TiO}_2(110)$.

Previous experimental studies have established that low-Miller-index faces of rutile TiO_2 form a range of stoichiometries, the nonstoichiometric phases being associated with O-vacancy (Ti^{3+}) creation. Such vacancies are thought to play a crucial role in determining the reactivity of oxide surfaces.² O vacancies are readily detectable on TiO_2 , as a d^1 band-gap state in photoemission spectra, providing a particular advantage in work which seeks to establish the influence of O vacancies. On the basis of experiments which have investigated the reactivity of O vacancies produced by different means (e.g., Ar-ion bombardment, thermal annealing), the influence of O vacancies on the surface chemistry of TiO_2 appears to be strongly dependent on their local geometry.² However, only now are details emerging of the surface crystallography, which are necessary in order to properly evaluate the structure and property relationship. In some cases, calculations of the energy-minimized structure are available for comparison.³⁻⁵

In terms of detailed surface crystallographic information, there are now extensive data on the nonstoichiometric $\text{TiO}_2(100)1 \times 3$ phase,⁶⁻¹⁰ and there are low-energy electron-diffraction (LEED) I - V results for the (001) surface.¹¹ Whereas the latter surface appears to

be close to bulk terminated, $\text{TiO}_2(100)1 \times 3$ is massively reconstructed. The form of this reconstruction has been studied by grazing incidence x-ray diffraction,⁶ photoelectron diffraction,⁷ and scanning tunneling microscopy (STM).⁸⁻¹⁰ The results indicate a microfacet reconstruction containing (110) planes, in which oxygen vacancies lie in the topmost layer of the selvedge.

The nonstoichiometric $\text{TiO}_2(100)1 \times 3$ phase is formed by thermal annealing in vacuum; formation of the corresponding 1×1 stoichiometric phase requires annealing in 10^{-6} -mbar O_2 . A similar behavior is observed in the case of the (110) surface, the subject of the present study. Here a stoichiometric 1×1 phase is formed either by annealing in O_2 or by annealing in vacuum at a temperature at which O diffuses from the bulk to quench surface O vacancies.¹²⁻¹⁷ Annealing at a lower temperature results in a nonstoichiometric 1×2 phase, which contains $\frac{1}{6}$ monolayer (ML) of O vacancies.¹⁴

The bulk-terminated structure of $\text{TiO}_2(110)$ which involves breaking the least number of bonds consists of alternative rows of fivefold-coordinated Ti^{4+} rows and bridging oxygen rows, as shown in Fig. 1(a). This model is consistent with the corresponding 1×1 LEED pattern of the stoichiometric surface¹² and with medium-energy electron-diffraction measurements.¹⁵ A simple model of the nonstoichiometric 1×2 phase was proposed on the basis of the Ti/O Auger peak ratio.¹⁴ In this model, which is shown in Fig. 1(b), alternate oxygen bridging rows in the 1×1 structure are removed.

An early STM study of $\text{TiO}_2(110)1 \times 1$ observed structures which were interpreted as the formation of O-vacancy-induced crystallographic shear planes.¹⁸ It was later suggested that these results represented an untypical area of the surface which is amenable to imaging.¹⁹ Two recent STM studies of the $\text{TiO}_2(110)1 \times 1$ and $(110)1 \times 2$

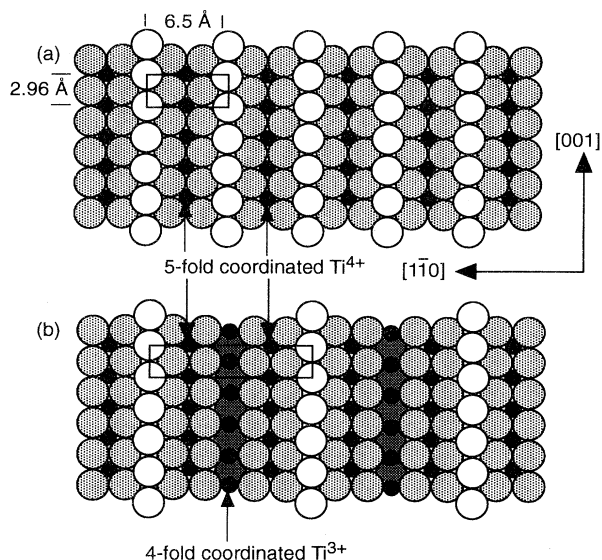


FIG. 1. (a) The standard model of stoichiometric $\text{TiO}_2(110)\text{-}1 \times 1$ (Ref. 2). Large circles represent O atoms, with the bridging O atoms shown as open circles; Ti atoms are represented by small filled circles. (b) The missing O-row model of $\text{TiO}_2(110)\text{-}1 \times 2$ (Refs. 2 and 14), in which alternate bridging O rows are removed from the stoichiometric 1×1 termination. Unit cells are outlined in both models.

phases^{16,17} obtained results which are consistent with the simple 1×1 structure shown in Fig. 1(a), with individual Ti atoms being resolved in one study.¹⁷ While there is agreement in their conclusions regarding the 1×1 phase, interpretation of the 1×2 -phase images is controversial.^{16,17} The model of Sander and Engel¹⁶ incorporates relaxation of the in-plane anions and cations into the model shown in Fig. 1(b), whereas Onishi and Iwasawa's model contains double ridges of a Ti_2O_3 -like structure.¹⁷ Additional features were observed by Sander and Engel¹⁶ having a local $c(2 \times 1)$ symmetry, being ascribed to a phase with the same O coverage as the 1×1 surface.

Recent theoretical studies which have calculated the energy-minimized structures of $\text{TiO}_2(110)$ (Refs. 3–5) predict a substantial relaxation of atoms perpendicular to the stoichiometric 1×1 and O-deficient 1×2 surface.²⁰ In one of these calculations a lateral relaxation of the in-plane O atoms on the stoichiometric 1×1 surface was also indicated.⁴

In this paper we describe the results of a STM study which has investigated four phases of $\text{TiO}_2(110)$ having a varying degree of O deficiency. The first corresponds to the stoichiometric 1×1 surface, our results being largely consistent with those previously published. The second phase is the nonstoichiometric 1×2 surface, for which our results are substantially better resolved than those previously published, leading us to propose a different structural model. The third phase is the $c(2 \times 1)$ superstructure¹⁶ which coexists with the 1×2 phase. In this work we find that this structure has a 2×2 local symmetry, and again we achieve higher resolution than in earlier work, the results pointing to a different structural model.

The fourth phase is a faceted structure, which contains some of the structure observed in the early STM study. Our data suggest that the results observed by Rohrer, Henrich, and Bonnell^{18,19} may have arisen from faceting rather than shear-plane formation.

II. EXPERIMENTAL DETAILS

All measurements were carried out in a UHV STM instrument (Omicron GmbH) which is equipped with facilities for argon-ion bombardment, LEED, retarding field Auger spectroscopy, and residual gas analysis. The base pressure of the instrument during these measurements was $\leq 10^{-10}$ mbar. Our STM instrument is designed for room-temperature operation, with the tip held at ground potential and the sample biased. Vertical and horizontal distances were calibrated using images of $\text{Cu}(110)2 \times 1\text{-O}$, for which the dimensions are known.²¹

Images were recorded in the constant current mode over a range of positive sample bias voltages and tunneling currents. As in previous work^{8–10} it did not prove possible to obtain images at negative sample bias reliably. Spectroscopy data were recorded by breaking the feedback loop, so as to maintain the tip at a constant height above the surface, while the bias voltage was ramped between the desired values.

The TiO_2 sample (Commercial Crystals Inc.) was cut and polished ($0.25 \mu\text{m}$) to within 0.5° of the (110) plane, as checked by Laue diffraction. It was vacuum reduced to introduce n -type conductivity ($\sim 10^{18} \text{ cm}^{-3}$). The sample was attached to a tantalum sample holder by spot-welded tantalum clips. This assembly was then rinsed in methanol and dried in N_2 gas before being inserted into the vacuum chamber via a load lock, where it was degassed for about 14 h. Cleaning of the sample *in situ* employed cycles of Ar-ion bombardment (500 eV, 4.5 μA drain current) and annealing to 1200 K. Annealing used an electron-beam heater, with electrons striking the back of the sample holder. Cleaning cycles were repeated until the crystal was judged to be clean and ordered using Auger spectroscopy and LEED, respectively. The sample temperature was monitored using a chromel-alumel thermocouple located approximately 2 cm from the sample. Additional Ar^+ bombardment and anneal cycles were used to reduce the seldedge progressively.

III. RESULTS AND DISCUSSION

A. The 1×1 stoichiometric surface

Figure 2 shows a typical STM image recorded at positive sample bias from the surface after initial cleaning. The corresponding LEED pattern has 1×1 symmetry. Under the conditions used to record this image, tunneling is into unoccupied states of the substrate, which have predominantly Ti 3d character.^{3–5} Hence features in the image will represent Ti atoms^{8–10,16–19} (all images reported in this paper were recorded under conditions which will image Ti atoms). Thin rows running parallel to [001] can be observed over most of the image in Fig. 2,

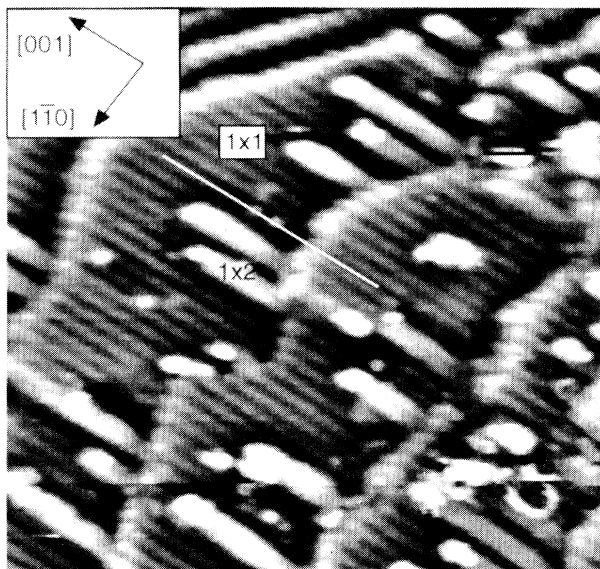


FIG. 2. A $200 \times 200\text{-}\text{\AA}^2$ STM image (+1 V, 1 nA) of $\text{TiO}_2(110)$, which contains mainly the 1×1 phase, observed as thin rows. Areas of the 1×2 phase can be seen growing out from step edges. The registry of the 1×1 rows across a step is highlighted by the white line drawn on the image.

as can a number of steps. In addition, a number of wider rows can be seen protruding from the step edges along $[001]$.

We first focus on the thin rows, which have an inter-row spacing of $6.5 \pm 0.1 \text{ \AA}$, the unit-cell dimension along $[\bar{1}\bar{1}0]$. In line with earlier work,^{16,17} we attribute these thin rows to fivefold-coordinated Ti atoms which are exposed on the 1×1 stoichiometric surface in the model shown in Fig. 1(a). The corrugation across these rows is measured from height profiles to be $0.3\text{--}0.5 \text{ \AA}$, depending on the tip and bias voltages used, again consistent with earlier work.¹⁷ Given the interpretation of the image in terms of the model in Fig. 1(a), this corrugation must be dominated by electronic effects, since geometry alone would produce a minimum at the Ti sites, with a maximum height on the bridging O rows. Height profiles across the steps which separate areas of the thin-row features indicate a step height of approximately 3 \AA , consistent with that expected for the 1×1 model in Fig. 1(a), 3.25 \AA .¹⁷ Moreover, the relationship between the thin rows on adjacent terraces is consistent with this model.¹⁷ These are offset by half a unit cell along $[\bar{1}\bar{1}0]$, as evidenced by the line drawn across a step in Fig. 2.

B. 1×2 structure at step edges

Turning now to the thicker rows visible in Fig. 2 at the step edges, which were also observed by Onishi and Iwasawa.¹⁷ The maximum separation measured between the centers of these rows is about 13 \AA , which indicates a doubling of the bulk unit cell along $[\bar{1}\bar{1}0]$. This structure is therefore consistent with a 1×2 reconstruction of the (110) surface. The relationship between images of the 1×2 phase and structural models is discussed in more de-

tail below. For the moment, we simply note that the thicker rows are more or less consistent with the model of the 1×2 phase shown in Fig. 1(b). They would arise from tunneling into the fivefold Ti sites which are also imaged on the 1×1 terraces, and fourfold sites which are nominally coplanar and which lie between the fivefold rows.

The relationship between the 1×2 rows and the 1×1 rows on the upper and lower terraces indicates that the 1×2 rows form part of the upper terraces. This is deduced from the comparison in Fig. 3 of a structural model of a step with a STM image. The latter indicates that the 1×2 wide row is in phase with the 1×1 rows of the upper terrace. From the model it can be seen that this is expected if the 1×2 row grows out from the upper ter-

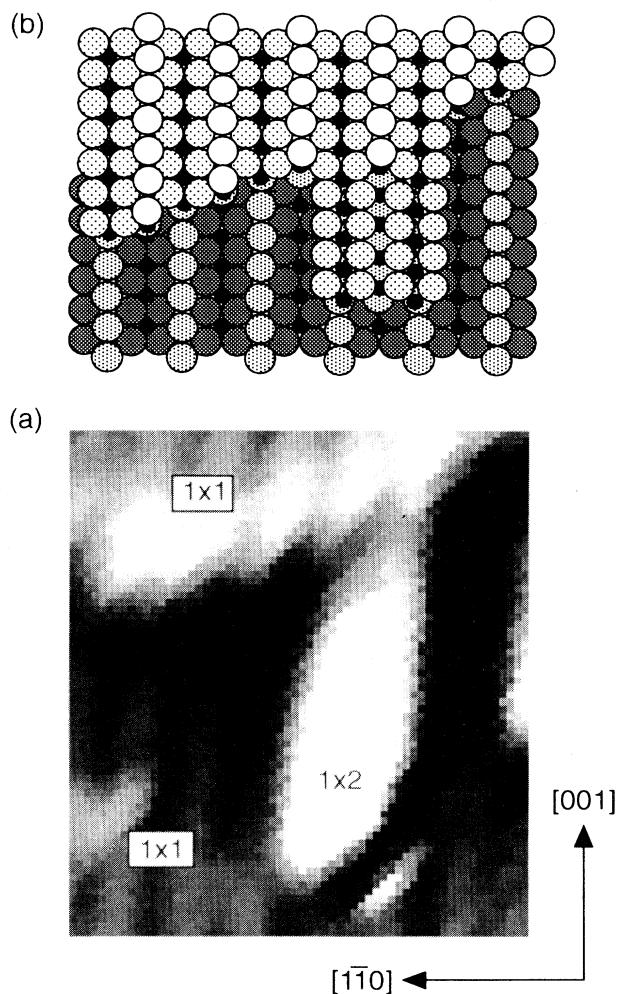


FIG. 3. (a) Expanded section of the image displayed in Fig. 2 which includes a 1×2 row growing out from a 1×1 step edge. The distance between 1×1 rows is 6.5 \AA . (b) Model of the 1×2 structure at 1×1 step edges, matched to the image in (a). Large circles represent O atoms, with lighter shading representing higher atoms. Small black circles represent Ti atoms.

race. The height of the 1×2 rows relative to the terraces is also in line with this model, being $2.5 \pm 0.1 \text{ \AA}$ above the lower terrace. The apparent $0.6 \pm 0.1 \text{ \AA}$ difference between the height of the 1×2 and 1×1 rows on the upper terrace could arise from either an electronic or a relaxation effect. As we show below, there does appear to be a lateral relaxation of fivefold-coordinated Ti atoms in the 1×2 phase, and this could be accompanied by a vertical relaxation. However, the results of recent calculations indicate that relaxation of the fivefold-coordinated Ti atoms are little affected by removal of adjacent bridging O rows.⁴

Both the 1×2 and 1×1 rows terminate in bright features. This can be explained on the basis of the reduced coordination number of Ti atoms at step edges, which are represented in Fig. 3(b). A significant modification of the electronic structure is expected to result from this change in geometry, which could increase the tunneling current at the bias voltage used. While a reduction to a Ti coordination number of 3 would explain the features observed at the step edges, it does not obviously explain the bright features which appear on the 1×1 rows where they transform to 1×2 rows. Here the bright features should correspond to fivefold-coordinated Ti. We tentatively suggest that in this case an enhanced tunneling current arises from local relaxation. Before moving on to discuss the 1×2 structure in more detail, we note that the model proposed by Onishi and Iwasawa¹⁷ to explain the interaction of 1×2 and 1×1 rows at step edges is quite different from that suggested here. This arises from a different interpretation of the 1×2 rows. In the earlier work¹⁷ the model proposed consists of raised ridges which are O terminated, with only a single exposed Ti row lying between them at a lower level. On the basis of the tunneling parameters used,¹⁷ one would expect to image predominantly Ti features.^{3-5,8-10,16-19} Two bright rows rather than one are observed for the 1×2 structure, hence there is an inconsistency between this earlier model and the data.

C. The 1×2 nonstoichiometric surface

The concentration of the 1×2 phase was enhanced in this work by further sputter and anneal cycles, resulting in the image shown in Fig. 4. The corresponding LEED pattern showed sharp integral order spots with streaking along the $[1\bar{1}0]$ direction. As in the image in Fig. 2, rows

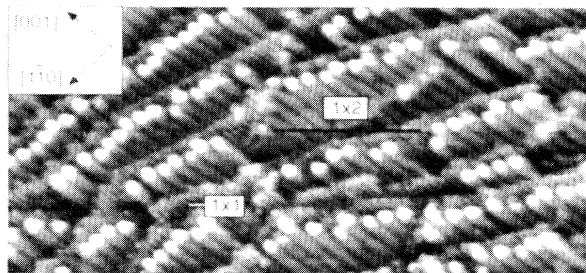


FIG. 4. A $500 \times 250 \text{-\AA}^2$ STM image ($+1.5 \text{ V}$, 1 nA) recorded after further reduction of the surface imaged in Fig. 2.

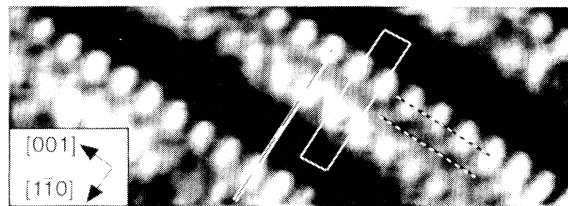


FIG. 5. A high-resolution $20 \times 50 \text{-\AA}^2$ differentiated STM image ($+1 \text{ V}$, 0.5 nA) of the 1×2 phase of $\text{TiO}_2(110)$. The apparent elongation of features on one side of the paired rows occurs in the scan direction, and is ascribed to a tip-related effect. The 1×2 unit cell is outlined. Height profiles from the undifferentiated image were taken from the lines indicated. Data from the $[1\bar{1}0]$ -direction line are used in Table I, while the $[001]$ -direction profiles are shown in Fig. 6.

having 1×1 and 1×2 periodicities can be seen running along $[001]$, with the 1×2 rows growing out of the 1×1 upper terraces. The only significant difference between the two images is that in Fig. 4 the 1×2 rows dominate.

A high-resolution image of the 1×2 phase is shown in Fig. 5, where the thick row is resolved into two parallel $[001]$ -direction rows in which features with atomic dimensions can be distinguished. The separation of these features along $[001]$ is approximately 3 \AA , consistent with the unit-cell dimension (2.96 \AA) in this direction. The distance between the atomic features in the perpendicular direction, $[1\bar{1}0]$, is $5.5 \pm 0.1 \text{ \AA}$. Weaker features are observed in the center of the unit cell marked on the image in Fig. 5, although they are not easily distinguished in the reproduced figure. For this reason, in Fig. 6 we compare line profiles in the $[001]$ direction across the bright atomically resolved row and across the weaker features. This comparison reveals the relative position of the two types of features, being offset by half a unit cell along $[001]$. Height profiles in the $[1\bar{1}0]$ direction along the line indicated in Fig. 5 are strongly dependent on the bias voltage and tunneling current, as shown in Table I. This is not surprising, since we are monitoring the difference between bridging O atoms, which form the dark areas, and Ti atoms, which give rise to the bright rows.

These data are almost consistent with the structural model for the 1×2 phase shown in Fig. 1(b), although

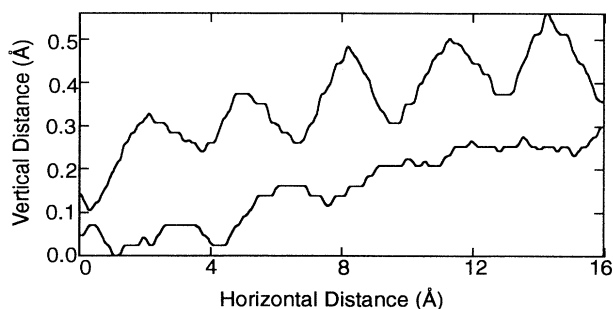


FIG. 6. Height profiles from the $[001]$ -direction lines in Fig. 5. The upper curve is for the bright row, while the lower curve is for the line which runs between the bright rows.

TABLE I. The difference in the apparent height of the bright and dark rows of the 1×2 structure as a function of the tunneling parameters. The corrugation heights were obtained from a height profile taken along the $[1\bar{1}0]$ -direction line indicated on Fig. 5.

Height (\AA)	Bias voltage (V)	Current (nA)
1.2	0.5	0.5
1.2	1.0	1.0
1.0	1.0	0.5
1.0	0.75	0.5
0.9	1.0	0.5
0.6	1.5	1.0
0.5	2.0	1.0

there are two significant discrepancies. One is the observed 5.5 ± 0.1 - \AA distance between Ti-atom rows along $[1\bar{1}0]$, which compares with the expected value of 6.5 \AA . The second is associated with the apparent height difference of the centered atoms compared to those on the bright rows, which should be coplanar [see Fig. 1(b)]. As can be seen from the height profiles in Fig. 6, what on the basis of the model in Fig. 1(b) should be the centered

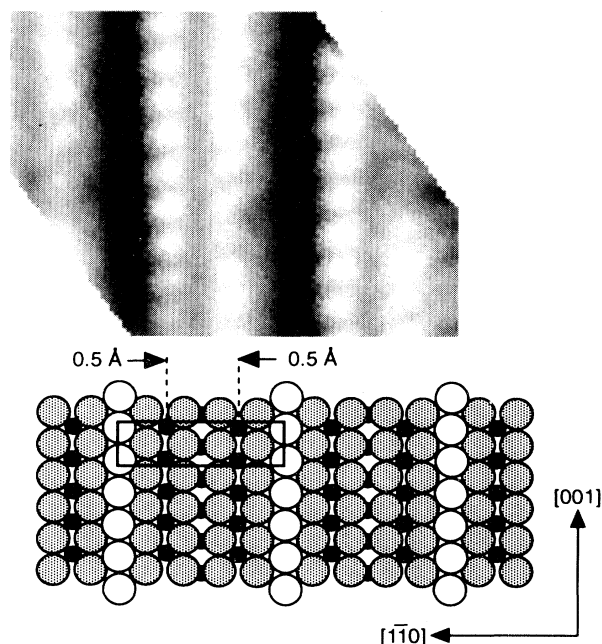


FIG. 7. Model of $\text{TiO}_2(110)-1 \times 2$ derived from the image in Fig. 5 and the line profiles shown in Fig. 6. A rotated section of the undifferentiated version of the image in Fig. 5 which is aligned and scaled to the model is included for clarity. Large open circles represent O atoms, and large shaded circles represent in-plane O atoms. Small black circles represent Ti^{4+} atoms, and small shaded circles represent Ti^{3+} atoms. The apparent misalignment of the O rows with the dark areas of the image is due to the elongation of Ti features on the right of the paired rows, which is ascribed to a tip-related effect. The fourfold-coordinated Ti atoms at the location of the O vacancies relax into the surface, while the fivefold-coordinated rows relax toward each other by 0.5 \AA . The 1×2 unit cell is outlined.

fourfold-coordinated Ti^{3+} ions appear to be about 0.25 \AA lower than the fivefold-coordinated Ti^{4+} species. This apparent height difference is not particularly sensitive to the tunneling conditions, although we cannot rule out a significant electronic structure contribution. Nevertheless, the height difference predicted by calculations, which arises from an inward relaxation of the fourfold sites by 0.2 \AA ,⁴ would be consistent with our measurements.

If we take the relaxation of the Ti^{3+} sites to be 0.2 \AA , then we can explain the discrepancy in the separation between rows along $[1\bar{1}0]$ by invoking a lateral relaxation of surface O atoms and the fivefold-coordinated Ti atoms. In order to explain the STM data, these Ti atoms must translate 0.5 \AA toward the missing bridging O row. The resulting structural model is compared with the STM image in Fig. 7. This model, which involves relatively subtle changes to the intuitive model proposed by Wu and Møller¹⁴ [see Fig. 1(b)], differs from those suggested on the basis of earlier STM data.^{16,17} The latter models were, however, based on data with insufficient resolution to distinguish individual features within the 1×2 wide rows.

D. 2×2 structure

A STM image obtained following a further sputter and anneal cycle is shown in Fig. 8. The corresponding LEED pattern was similar to that observed for the 1×2 structure discussed in Sec. III C. A number of steps are observed in the image, with the ends of the 1×2 rows terminating in bright spots consistent with the images presented above. Line profiles show the step height between areas of 1×2 to be 3.2 ± 0.1 \AA , in agreement with

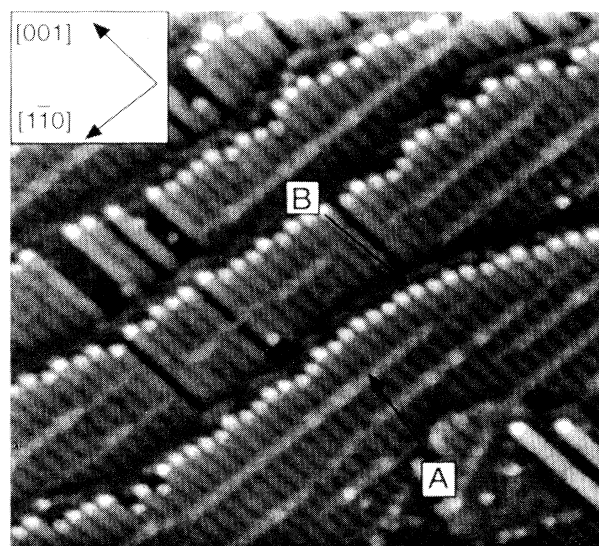


FIG. 8. A 500×500 - \AA^2 STM image ($+1$ V, 1 nA) of $\text{TiO}_2(110)$ recorded after further reduction of the surface imaged in Fig. 4. The majority phase is still 1×2 , but rows perpendicular to the 1×2 rows are now observed, annotated as A. In addition, a ledge between 1×2 terraces is indicated (B).

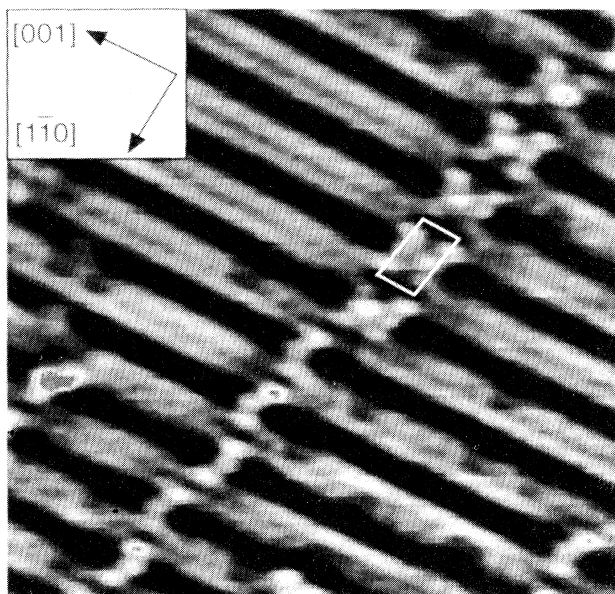


FIG. 9. A higher-resolution $80 \times 100 \text{ \AA}^2$ STM image (+0.5 V, 0.5 nA) of an area of Fig. 8. The 2×2 unit cell is indicated.

the expected value of 3.25 \AA . Furthermore, the dark lines associated with bridging oxygen are displaced along $[1\bar{1}0]$ by half a unit cell distance over a step, again in agreement with the rutile step structure. A layer can be seen jutting out between the upper and lower terraces, which line profiles indicate are 2.5 \AA below the upper terrace. This is consistent with the measurements from Fig. 3 of the difference between 1×2 and 1×1 phases on adjacent terraces. Hence we associate these ledges with remaining areas of 1×1 which have not been transformed to 1×2 .

In addition to the 1×2 phase, another structure is observed in Fig. 8, which consists of rows perpendicular to the 1×2 rows. This structure was also observed by Sander and Engel.¹⁶ The spacing of these $[1\bar{1}0]$ -direction rows varies from 25 to 50 \AA . A higher-resolution image of the $[1\bar{1}0]$ -direction rows is shown in Fig. 9. From this image it is apparent that the rows are comprised of either

single or double strands of three features located in the vicinity of the gaps between the 1×2 paired rows. By reference to Fig. 7, this corresponds to the position of the remaining bridging O rows. The middle of the three features in each strand is centered between the other two features along $[1\bar{1}0]$, and is offset from them by about 1.5 \AA along $[001]$, forming a triangle. In double strands the features are arranged so that the two triangles point toward each other, although on single strands there appears to be no preferential orientation. In addition to the features observed in the gaps between 1×2 double rows, the adjacent section of the 1×2 rows appears darker. The $[001]$ -direction separation of the bright features which lie close to one of the 1×2 double rows is measured to be $5.9 \pm 0.1 \text{ \AA}$, which corresponds to two unit cells in this direction. The measured separation along $[1\bar{1}0]$ between the bright features either side of the 1×2 rows is $6.5 \pm 0.1 \text{ \AA}$, consistent with the bulk-terminated unit-cell length in this direction. In a double strand, the separation along $[001]$ of the features seen centered on gaps between 1×2 double rows is measured to be $3.0 \pm 0.1 \text{ \AA}$, corresponding to one unit cell in this direction (2.96 \AA). Overall, this indicates a double strand structure which has 2×2 local symmetry, and which is periodic along $[1\bar{1}0]$.

The earlier assertion that cations are imaged at positive sample bias leads to the assignment of the strands as Ti atoms. This is supported by a comparison of scanning tunneling spectroscopy (STS) data recorded from parts of the image shown in Fig. 9. In earlier work it has been shown that for this relatively ionic material it is possible to use STS to distinguish between cation and anion sites.⁹ This relies on the mainly O $2p$ character of the valence band, which is separated by a band gap of about 3 eV from the mainly Ti $3d$ conduction band. The spectroscopy data from $\text{TiO}_2(110)-1 \times 2$ are shown in Fig. 10. One spectrum was recorded from the dark region between 1×2 double rows, which corresponds to the position of a bridging O row; the second shows data measured on one of the 1×2 rows, corresponding to fivefold-coordinated Ti atoms; the third was taken from a sum of all three features of the $[1\bar{1}0]$ -direction row.

The three spectra are similar at positive bias, which is to be expected given the stabilization conditions (+1 V, 1

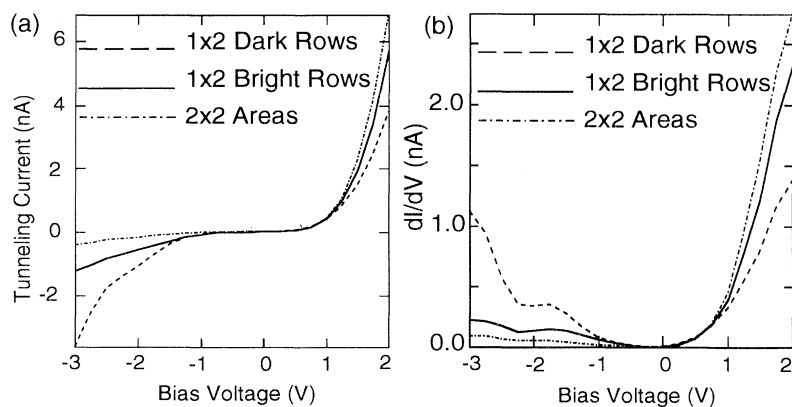


FIG. 10. (a) STS spectra recorded from different parts of the image in Fig. 9, after stabilizing the tip at +1 V, 1 nA. (b) The corresponding differential conductance spectra.

nA). However, there is a marked difference between them at negative bias. The spectrum recorded from the bridging O rows has the highest contribution to the negative-bias tunneling current. This is indicative of a high density of occupied states and is in line with our expectations. By comparison, the negative-bias tunneling current from the fivefold-coordinated Ti atoms and features of the $[1\bar{1}0]$ -direction row is small. This indicates that the bright features in the $[1\bar{1}0]$ -direction strands represent Ti atoms.

Figure 11 contains a structural model of the double strand 2×2 and the single strand superlattices which are consistent with the image in Fig. 9 and the spectroscopy data. For clarity, in Fig. 11 the model is compared with a section of Fig. 9. In the model, which has the same O-vacancy density as the 1×2 phase, the bright features which lie between the 1×2 double rows are created by removing O atoms from the bridging-O row to expose Ti atoms. For the double strand structure, three atoms are moved from the bridging O row to occupy atop sites on two adjacent fivefold-coordinated Ti sites and to reoccupy a missing-bridging row site. Moving O atoms to these sites explains the dark areas within the 1×2 double row adjacent to the bright features. An integral part of this

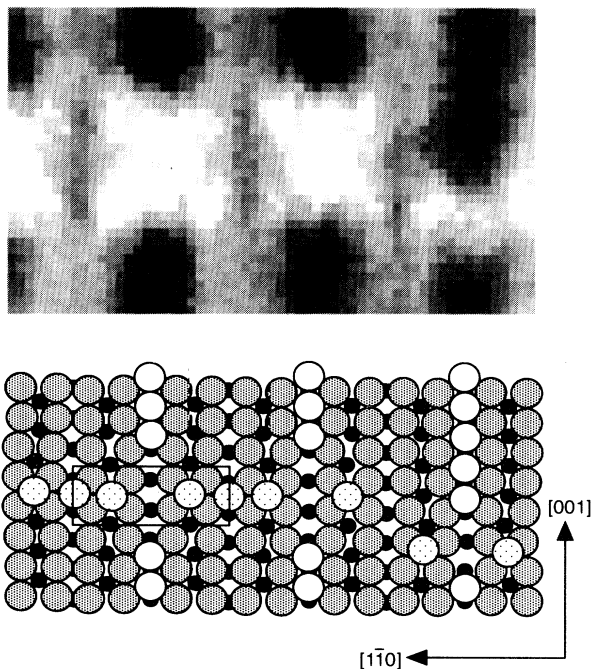


FIG. 11. Model of the 2×2 phase based on the image in Fig. 9 and the STS spectra in Fig. 10. A rotated section of the image of Fig. 9 which is aligned and scaled to the model is included for clarity. The left-hand side of the image and model contain a double strand of the 2×2 superlattice, while the right-hand side contains a single strand. Ti atoms are represented by small circles, those which are lightly shaded are associated with the 2×2 structure. Large circles represent oxygen atoms, with bridging oxygens shown as open circles, hopping oxygen atoms as lightly shaded circles, and in-plane oxygen atoms as heavily shaded circles. The 2×2 unit cell is indicated.

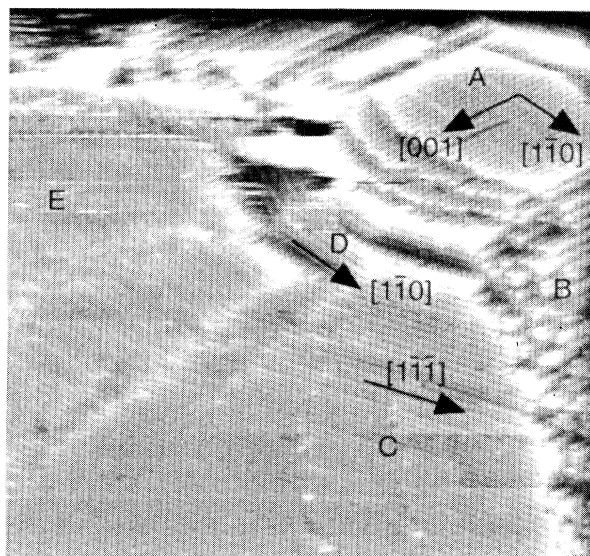


FIG. 12. A large area $1000\times 1000\text{-}\text{\AA}^2$ STM image ($+0.5\text{ V}$, 0.5 nA) of $\text{TiO}_2(110)$ recorded after further reduction of the surface imaged in Fig. 8. This image has been high pass filtered to accommodate the large height difference across the image (140 \AA). An area of the $1\times 2+2\times 2$ phase can be seen in the top right hand corner of the image [A], while the remainder of the image contains facets of (100) [B], (101) [C], (111) [D], and (011) [E] planes.

model is the relaxation of fivefold Ti atoms on the 1×2 double row which form part of the strands back to their 1×1 positions. This explains why the associated bright features appear to be shifted slightly away from the 1×2 rows along $[1\bar{1}0]$. As for the single strands, a similar model explains the images, in which only two O atoms are moved from the bridging O row, with the hopping oxygen atoms located on adjacent fivefold Ti atoms displaced by half a unit cell from the exposed fourfold atom toward either $[001]$ or $[00\bar{1}]$. That a displacement in either direction should result in the same surface energy is consistent with the observed random orientation of the single strands.

The STM images and associated models illustrate the 2×2 local symmetry of the double strands, which are periodic along $[1\bar{1}0]$. The model of this structure is at odds with that suggested by Sanders and Engel.¹⁶ This discrepancy arises principally from the difference in the model of the underlying 1×2 structure derived in the two studies. While the 2×2 structure can be explained in terms of a structural model, a definitive explanation for its occurrence cannot be provided. However, it seems likely that it is related to the strain imposed by the lateral translation of fivefold-coordinated sites in the 1×2 phase. Formation of the 2×2 superlattice would act to relieve this strain and hence lower the surface energy.

E. Faceting

A further five sputter and anneal cycles resulted in a surface which gave a LEED pattern which had a high background and showed streaking in both $[001]$ and

$[1\bar{1}0]$ directions between the integral order beams. A large area image of this surface is shown in Fig. 12, which has been high pass filtered to compensate for the large dynamic range (140 Å). Extensive faceting is evidenced, with only the top right hand corner of the image, annotated as *A*, containing structures corresponding to the 1×2 and 2×2 phases.

Inspection of the overall morphology indicates that there are facets of the (100) (*B*), (101) (*C*), (111) (*D*), and (011) (*E*) planes. These were identified by noting the rotation of the facet surface normals to $[110]$, using raw data to avoid effects introduced by image processing. The angle between the planes defined by *A* and *B* is measured to be $46\pm 4^\circ$, the facet normal being rotated toward $[1\bar{1}0]$, consistent with *B* being a (100) plane. The surface normal to the *C* facet lies $62\pm 5^\circ$ away from the $[1\bar{1}0]$ direction in the (110) plane and $55\pm 5^\circ$ away from the (110) surface normal. This is consistent with the area labeled *C* being a (101) plane. The area labeled *D* corresponds to a (111) plane, given that the rows seen in this plane are parallel to the $[1\bar{1}0]$ direction, with the facet surface normal rotated $60\pm 6^\circ$ from $[110]$ toward $[001]$. The area labeled *E* corresponds to a (011) plane, the rows being orientated $62\pm 6^\circ$ away from $[001]$, with the facet surface normal being rotated by $52\pm 7^\circ$ from $[110]$ toward $[1\bar{1}0]$. Other facets are observed in the upper part of the image in Fig. 12, although it is difficult to determine their precise location.

The observation of facets containing $\{111\}$ and $\{011\}$ planes is consistent with studies of $\text{TiO}_2(001)$ faceting, in which the same planes were evidenced.²²⁻²⁴ The (100) plane contained in area *B* has $[001]$ -direction rows separated by about 14 Å, in line with that expected on the basis of STM images of $\text{TiO}_2(100)1\times 3$.⁸⁻¹⁰ On this surface, which contains $\frac{1}{3}$ ML of O vacancies, the 14-Å periodicity arises from a reconstruction which involves formation of (110) microfacets, which on the surface imaged here should lie parallel and perpendicular to the macroscopic surface.

Before considering the structure of the (101) facet in more detail, we briefly compare our results to those of a previous electron stimulated ion angular distribution (ESDIAD) study.¹³ The ESDIAD patterns from $\text{TiO}_2(110)$ with a higher O-vacancy density were attributed to the formation of steps of high index planes.¹³ In that at least one of the facets observed here, the $(100)1\times 3$ plane, has double the O-vacancy density of the $(110)1\times 2$ surface is consistent with the ESDIAD work.

We turn now to the (101) facets which contain $[1\bar{1}\bar{1}]$ -direction rows. Structures similar to that observed on the facets were observed in an early STM study of a

$\text{TiO}_2(110)$ surface which displayed a 1×1 LEED pattern.¹⁸ In this early work, rows separated by 8.5 Å were observed to run in what was assigned to the $[1\bar{1}\bar{1}]$ direction, being ascribed to the result of crystallographic shear-plane formation. However, because the crystal axis system chosen was one in which the $[110]$ direction points into the bulk, the rows are equivalent to those observed here. The measurements here indicate an inter-row separation of 9 ± 1 Å, in line with the earlier study. Our results therefore suggest that the shear-plane structures observed in the earlier work^{18,19} arise simply from faceting.

IV. CONCLUSIONS

In summary, we have used STM to investigate the structure of four phases of $\text{TiO}_2(110)$. The results are consistent with imaging Ti atoms, as expected given the positive sample bias employed. It has been possible to deduce structural models for all of these phases, one of which is stoichiometric (1×1), two of which are reduced phases (1×2 and 2×2), and one of which involves faceting.

While the structure of 1×1 phase derived here is consistent with that arrived at in earlier studies,^{16,17} structures of the 1×2 and 2×2 phases differ markedly from those previously suggested.^{16,17} This arises from the higher resolution obtained for the 1×2 phase, on which our model for the 2×2 phase is based. Conversion of the 1×1 to the 1×2 phase involves removing alternate bridging O rows, with an accompanying lateral relaxation of fivefold-coordinated Ti atoms and a downward relaxation of fourfold Ti atoms. The 2×2 structure is periodic only along $[1\bar{1}0]$, its formation possibly being associated with the relief of strain imposed by the 1×2 morphology. This 2×2 phase has the same O-vacancy density as that of the 1×2 , but O atoms move from the remaining bridging O rows to reoccupy sites on the missing bridging O rows and to occupy atop sites on fivefold Ti atoms. Further reduction of the surface leads to faceting on the surface. One of the facets contains $[1\bar{1}\bar{1}]$ -direction rows. Such rows were observed in a previous study,^{18,19} where their presence was ascribed to crystallographic shear-plane formation. The results presented here suggest an alternative origin, namely that the substrate studied in the earlier work was faceted.

ACKNOWLEDGMENTS

We are grateful to F. M. Leibsle for useful discussions. This work was funded by the United Kingdom Engineering and Physical Sciences Research Council.

*Also at Department of Chemistry, University of Manchester, Manchester M13 9PL, United Kingdom.

¹A. Fujishima and K. Honda, *Nature* **238**, 37 (1972).

²V. E. Henrich and P. A. Cox, *The Surface Science of Metal Oxides* (Cambridge University Press, Cambridge, 1994).

³D. Vogtenhuber, R. Podlucky, A. Neckel, S. G. Steinemann, and A. J. Freeman, *Phys. Rev. B* **49**, 2099 (1994).

⁴M. Ramamoorthy, R. D. King-Smith, and D. Vanderbilt, *Phys. Rev. B* **49**, 7709 (1994).

⁵M. Ramamoorthy, D. Vanderbilt, and R. D. King-Smith, *Phys.*

- Rev. B **49**, 16721 (1994).
- ⁶P. Zschack, J. B. Cohen, and Y. W. Chung, Surf. Sci. **262**, 395 (1991).
- ⁷P. J. Hardman, N. S. Prakash, C. A. Muryn, G. N. Raikar, A. G. Thomas, A. F. Prime, G. Thornton, and R. J. Blake, Phys. Rev. B **47**, 16056 (1993).
- ⁸G. W. Clarke and L. L. Kesmodel, Ultramicroscopy **41**, 77 (1992).
- ⁹P. W. Murray, F. M. Leibsle, H. J. Fisher, C. F. J. Flipse, C. A. Muryn, and G. Thornton, Phys. Rev. B **46**, 12877 (1992).
- ¹⁰P. W. Murray, F. M. Leibsle, C. A. Muryn, H. J. Fisher, C. F. J. Flipse, and G. Thornton, Phys. Rev. Lett. **72**, 689 (1994).
- ¹¹C. G. Mason, S. P. Tear, T. N. Doust, and G. Thornton, J. Phys. Condens. Matter **3**, S97 (1991).
- ¹²V. E. Henrich and R. L. Kurtz, Phys. Rev. B **23**, 6280 (1981).
- ¹³R. L. Kurtz, Surf. Sci. **177**, 526 (1986).
- ¹⁴P. J. Møller and M. C. Wu, Surf. Sci. **224**, 265 (1989).
- ¹⁵B. L. Maschhoff, J. M. Pan, and T. E. Madey, Surf. Sci. **259**, 190 (1991).
- ¹⁶M. Sander and T. Engel, Surf. Sci. **302**, L263 (1994).
- ¹⁷H. Onishi and Y. Iwasawa, Surf. Sci. **313**, L783 (1994).
- ¹⁸G. S. Rohrer, V. E. Henrich, and D. A. Bonnell, Science **250**, 1239 (1990).
- ¹⁹G. S. Rohrer, V. E. Henrich, and D. A. Bonnell, Surf. Sci. **278**, 146 (1992).
- ²⁰In Ref. 4 the 1×2 indices are reversed from normal convention.
- ²¹D. J. Coulman, J. Winterlin, R. J. Behm, and G. Ertl, Phys. Rev. Lett. **64**, 1761 (1990).
- ²²R. H. Tait and R. V. Kasowski, Phys. Rev. B **20**, 5178 (1979).
- ²³L. E. Firment, Surf. Sci. **116**, 205 (1982).
- ²⁴G. E. Poirier, B. K. Hance, and J. M. White, J. Vac. Sci. Technol. B **10**, 6 (1992).

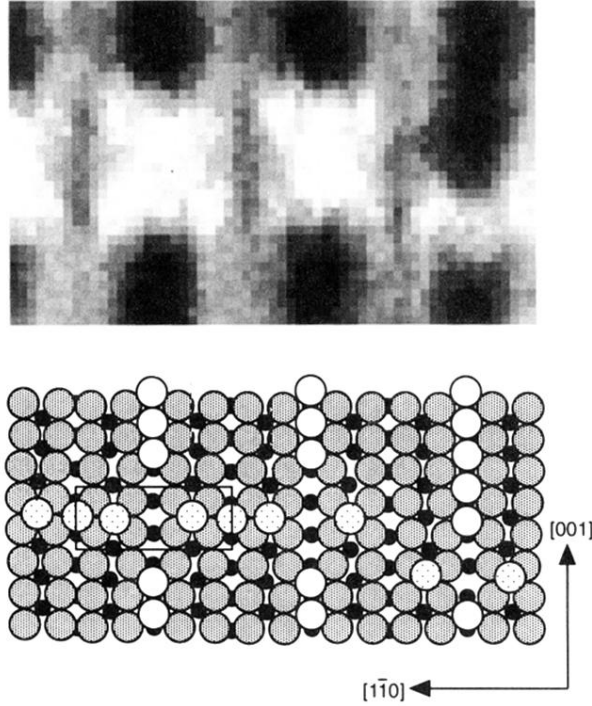


FIG. 11. Model of the 2×2 phase based on the image in Fig. 9 and the STS spectra in Fig. 10. A rotated section of the image of Fig. 9 which is aligned and scaled to the model is included for clarity. The left-hand side of the image and model contain a double strand of the 2×2 superlattice, while the right-hand side contains a single strand. Ti atoms are represented by small circles, those which are lightly shaded are associated with the 2×2 structure. Large circles represent oxygen atoms, with bridging oxygens shown as open circles, hopping oxygen atoms as lightly shaded circles, and in-plane oxygen atoms as heavily shaded circles. The 2×2 unit cell is indicated.

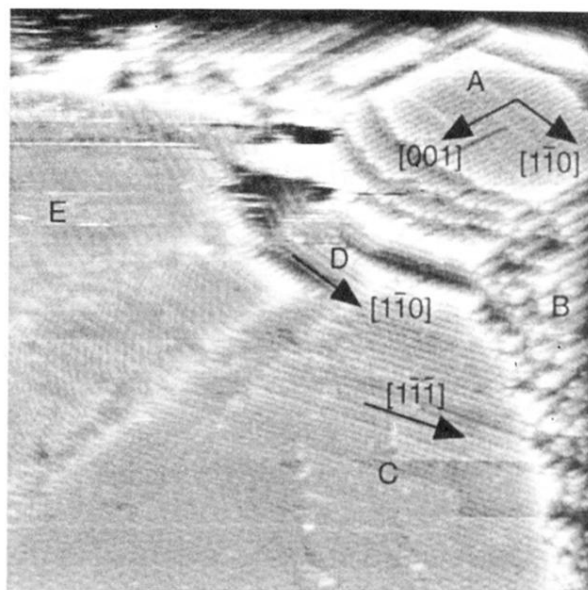


FIG. 12. A large area $1000 \times 1000 \text{ \AA}^2$ STM image (+0.5 V, 0.5 nA) of $\text{TiO}_2(110)$ recorded after further reduction of the surface imaged in Fig. 8. This image has been high pass filtered to accommodate the large height difference across the image (140 \AA). An area of the $1 \times 2 + 2 \times 2$ phase can be seen in the top right hand corner of the image [A], while the remainder of the image contains facets of (100) [B], (101) [C], (111) [D], and (011) [E] planes.

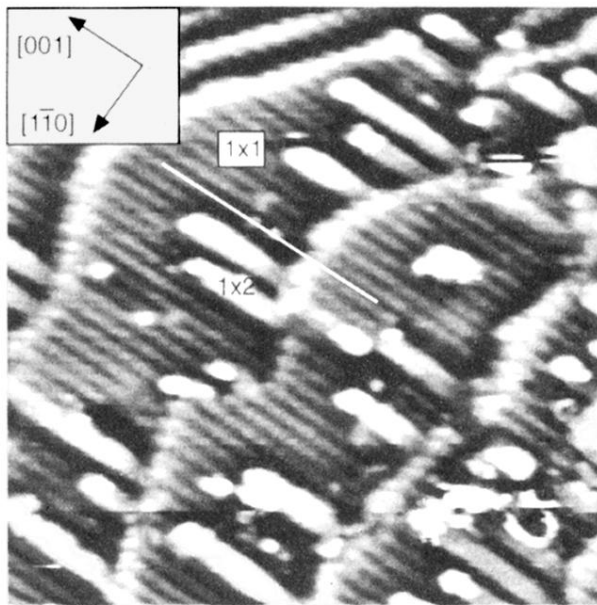


FIG. 2. A $200 \times 200 \text{ \AA}^2$ STM image (+1 V, 1 nA) of $\text{TiO}_2(110)$, which contains mainly the 1×1 phase, observed as thin rows. Areas of the 1×2 phase can be seen growing out from step edges. The registry of the 1×1 rows across a step is highlighted by the white line drawn on the image.

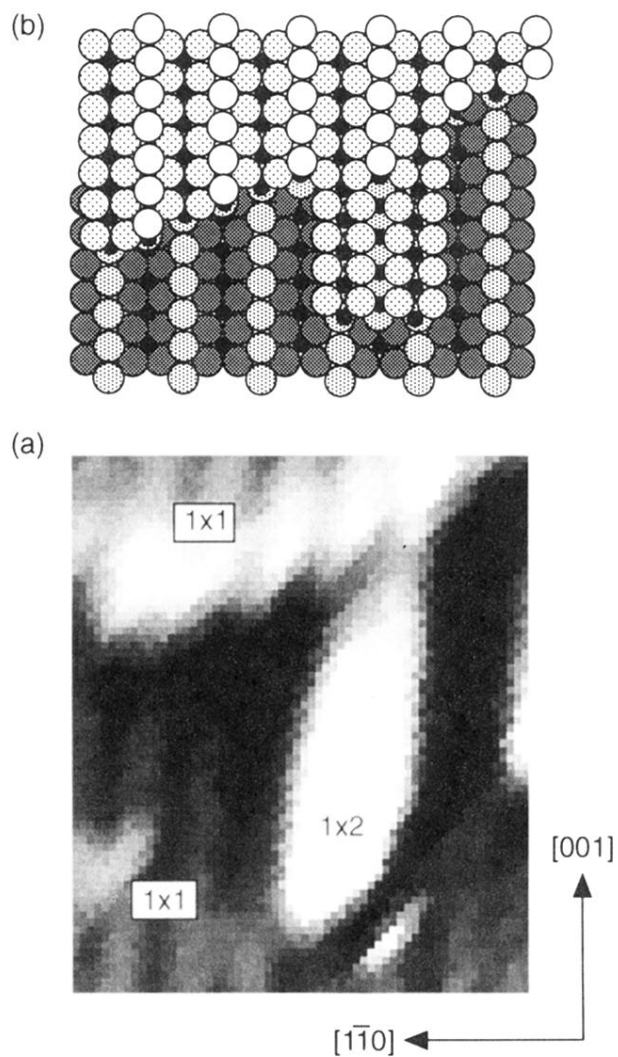


FIG. 3. (a) Expanded section of the image displayed in Fig. 2 which includes a 1×2 row growing out from a 1×1 step edge. The distance between 1×1 rows is 6.5 \AA . (b) Model of the 1×2 structure at 1×1 step edges, matched to the image in (a). Large circles represent O atoms, with lighter shading representing higher atoms. Small black circles represent Ti atoms.

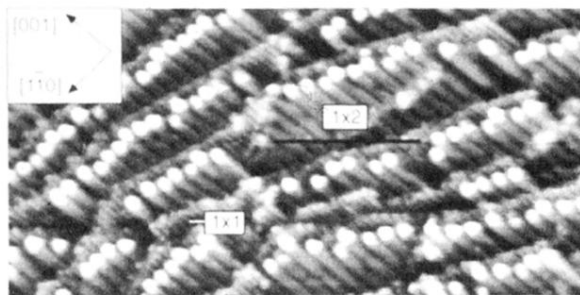


FIG. 4. A $500 \times 250\text{-\AA}^2$ STM image (+1.5 V, 1 nA) recorded after further reduction of the surface imaged in Fig. 2.

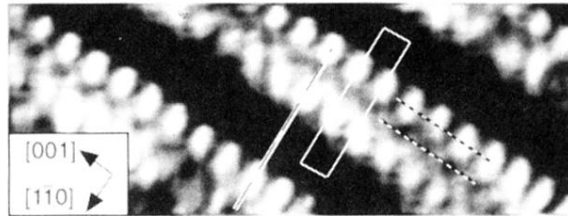


FIG. 5. A high-resolution $20 \times 50\text{-\AA}^2$ differentiated STM image (+1 V, 0.5 nA) of the 1×2 phase of $\text{TiO}_2(110)$. The apparent elongation of features on one side of the paired rows occurs in the scan direction, and is ascribed to a tip-related effect. The 1×2 unit cell is outlined. Height profiles from the undifferentiated image were taken from the lines indicated. Data from the $[1\bar{1}0]$ -direction line are used in Table I, while the $[001]$ -direction profiles are shown in Fig. 6.

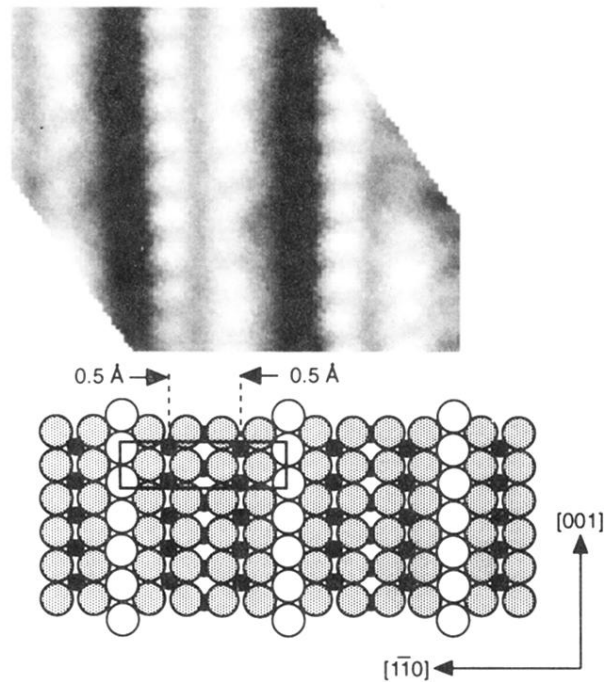


FIG. 7. Model of $\text{TiO}_2(110)\text{-}1\times 2$ derived from the image in Fig. 5 and the line profiles shown in Fig. 6. A rotated section of the undifferentiated version of the image in Fig. 5 which is aligned and scaled to the model is included for clarity. Large open circles represent O atoms, and large shaded circles represent in-plane O atoms. Small black circles represent Ti^{4+} atoms, and small shaded circles represent Ti^{3+} atoms. The apparent misalignment of the O rows with the dark areas of the image is due to the elongation of Ti features on the right of the paired rows, which is ascribed to a tip-related effect. The fourfold-coordinated Ti atoms at the location of the O vacancies relax into the surface, while the fivefold-coordinated rows relax toward each other by 0.5 \AA . The 1×2 unit cell is outlined.

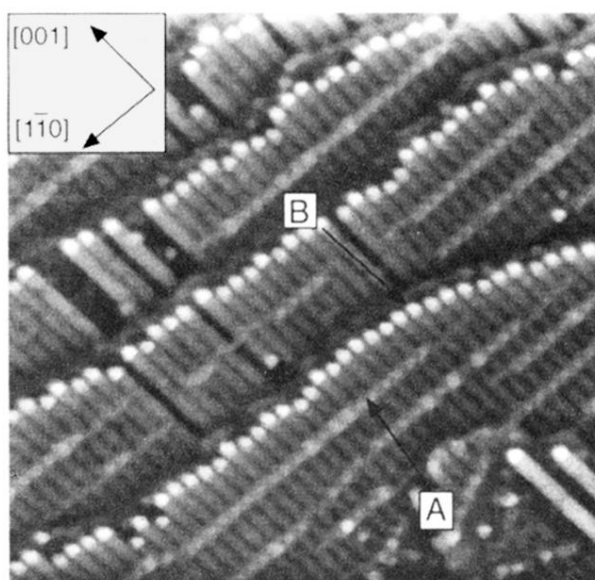


FIG. 8. A $500 \times 500 \text{ \AA}^2$ STM image (+ 1 V, 1 nA) of $\text{TiO}_2(110)$ recorded after further reduction of the surface imaged in Fig. 4. The majority phase is still 1×2 , but rows perpendicular to the 1×2 rows are now observed, annotated as *A*. In addition, a ledge between 1×2 terraces is indicated (*B*).

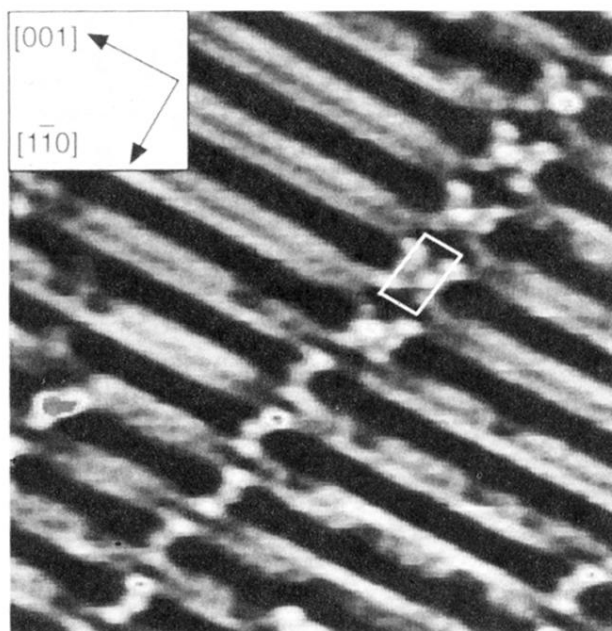


FIG. 9. A higher-resolution $80 \times 100\text{-\AA}^2$ STM image (+0.5 V, 0.5 nA) of an area of Fig. 8. The 2×2 unit cell is indicated.